ARTICLES SCIENCE CHINA Materials

mater.scichina.com link.springer.com

Published online 5 November 2018 | https://doi.org/10.1007/s40843-018-9359-7

Sci China Mater 2019, 62(5): 624–632

N-doped carbon-coated Co_3O_4 nanosheet array/carbon cloth for stable rechargeable Zn-air batteries

Qi Liu, Lei Wang*, Xu Liu, Peng Yu, Chungui Tian and Honggang Fu*

ABSTRACT **Although the application of various non-precious compounds as the air cathodes of Zn-air batteries has been explored, the construction of highly efficient self-supported Co-based electrodes remains challenging and highly desired given their outstanding electrocatalytic activity and cost-effectiveness. Herein, we fabricated a three-dimensional (3D) self-supported electrode based on N-doped, carbon-coated Co_3O_4 nanosheets grown on a carbon cloth (i.e., NC-Co_3O_4/CC) through the electrochemical deposition and carbonization. When used as a binder-free electrode for oxygen evolution reaction (OER), the NC–Co_3O_4/CC electrode demonstrated excellent electrocatalytic activity with an overpotential of 210 mV at 10 mA cm^{-2} and a Tafel slope of 79.6 mV dec^{-1}. In the Zn-air battery test, the electrode delivered a small charge/discharge voltage gap (0.87 V at 10 mA cm^{-2}) and exhibited high durability without degradation after 93 cycles at the large current density of 25 mA cm^{-2}. The durability of our electrode was superior to that of a commercial Pt/C+RuO_2 catalyst. The excellent performance of NC–Co_3O_4/CC could be attributed to the presence of 3D structures that promoted electron/ion transfer. By the absence of a binder, the carbon coating improved electron conductivity and promoted electrochemical stability. Moreover, N doping could be used to adjust the C electron structure and accelerate electron transfer. The present study provides a facile and effective route for the synthesis of various self-supported electrodes that fulfill the requirements of different energy storage and conversion devices.**

Keywords: N-doped carbon, Co_3O_4 nanosheet, self-supported electrode, oxygen evolution reaction, Zn-air batteries

INTRODUCTION

Energy demand has grown as living standards of humans continue to improve [1–3]. The use of traditional fossil fuels with low energy efficiency has resulted in a series of problems, such as global warming and environmental pollution [4,5]. Thus, unremitting efforts have been attempted to the development of new types of high-performance energy storage and conversion devices that are based on clean, energy-intensive, and sustainable sources instead of conventional fossil fuels [6–8]. Rechargeable Zn-air batteries stand out among novel storage and conversion devices because of their high theoretical energy density of 1,084 W h kg^{-1}, low cost, fine safety, and environmental friendliness [9–11]. The performance of air cathodes during charging, however, is degraded due to the high charging overpotential of Zn-air batteries that results from the sluggish kinetics of oxygen evolution reaction (OER) [12–14]. Precious metal-based catalysts, such as IrO_2 and RuO_2 are regarded as state-of-the-art OER electrocatalysts with high activity, but they are generally plagued with high cost, limited reserves, and poor durability [15,16]. Therefore, the development of high-efficiency OER catalysts with accelerated kinetic processes and superior durability from inexpensive and abundant earth elements has become the top priority of researchers, aiming to boost the overall performance of Zn-air batteries [17–19].

Currently, first-row transition metal compounds, such as Fe, Co, Ni, and Mn oxides [20–22]; (oxy)hydroxides [23,24]; phosphides [25]; sulfides [26–30]; and nitrides [31,32] are extensively studied as non-precious OER catalysts to replace the expensive IrO_2 and RuO_2 [33,34]. Co_3O_4 is a highly promising candidate as an OER catalyst because of its excellent electrocatalytic activity. Moreover, it can be easily handled [35]. Nanostructures with various morphologies, including nanosheets, nanofibers, nanowires, and nanoparticles, have been employed as OER catalysts. Three-dimensional (3D) nanostructures are highly favored because of their structural advantages [36–38]. Catalyst stability could also be improved through

Key Laboratory of Functional Inorganic Material Chemistry, Ministry of Education of the People's Republic of China, Heilongjiang University, Harbin 150080, China

* Corresponding authors (emails: fuhg@vip.sina.com, fuhg@hlju.edu.cn (Fu H); wanglei0525@126.com (Wang L))

the introduction of carbon nanostructures [39]. Nanostructure-based catalysts are fabricated as films and pasted on the surfaces of electrodes with a binder to block the transfer and diffusion of electrons, electrolytes, and gas by increasing the resistance and plugging active sites [40,41]. Alternatively, self-supported conductive substrates can be used to solve the above problems successfully [42]. Electrochemical processes could be stabilized by the strong synergistic interactions between the active materials and conductive substrates of Co_3O_4 nanostructures grown *in situ*.

In this study, 3D N-doped carbon-coated Co_3O_4 nanosheets grown *in situ* on carbon cloth (NC-Co_3O_4/CC) was constructed through a simple strategy that combined electrochemical deposition and carbonization. This 3D structure is designated as NC–Co_3O_4/CC chemically. During synthesis, $Co(OH)_2$ nanosheets were first grown on the CC in cobalt salt aqueous solution *via* electrodeposition and then converted to Co_3O_4 nanosheets through calcination. Then, NC–Co_3O_4/CC was formed by uniformly coating Co_3O_4 nanosheets with N-doped carbon derived from dicyandiamide. When used as a binder-free electrode for OER, the optimized NC–Co_3O_4/CC-600 exhibited an overpotential of 210 mV at a current density of 10 mA cm^{-2} and a Tafel slope of 79.6 mV dec^{-1} in 1.0 mol L^{-1} O_2-saturated KOH electrolyte. The assembled rechargeable Zn-air battery with NC–Co_3O_4/CC-600 air cathode showed small charge/discharge voltage gap and excellent durability even under large current density. The durability of the Zn-air battery with NC–Co_3O_4/CC-600 was superior to that of the commercial Pt/C+RuO_2 electrode. Our study offers an effective strategy for the design of high-performance air-cathode catalysts for rechargeable Zn-air batteries.

EXPERIMENTAL SECTION

Synthesis

CC substrates were first boiled in acetone for 20 min and then immersed for 30 min in 1.0 mol L^{-1} HCl aqueous solution under sonication. The as-treated CC substrates were collected after washing with deionized water and drying at 60°C in a vacuum oven overnight. The 3D $Co(OH)_2$/CC composite was synthesized using a common electrodeposition strategy, wherein 0.1 mol L^{-1} $Co(NO_3)_2$ was used as the electrolyte. The as-treated CC (2 cm× 2 cm), a saturated calomel electrode (SCE), and a Pt plate with a size of 1 cm^2 were used as the working electrode, reference electrode, and counter electrode, respectively. Electrodeposition was performed for different durations at 1.0 V; samples that were subjected to 600, 900, and 1,200 s of electrodeposition were designated as $Co(OH)_2$/CC-600, $Co(OH)_2$/CC-900, and $Co(OH)_2$/CC-1200, respectively. The synthetic $Co(OH)_2$/CC composite was calcined in a muffle furnace at 400°C for 2 h at a heating rate of 2°C min^{-1} to obtain Co_3O_4/CC composites. The carbon resource solution was prepared by dissolving 1.5 g of dicyandiamide in 70 mL of deionized water. The Co_3O_4/CC composite was then immersed for 24 h in the carbon resource solution. Subsequently, the dicyandiamide-coated Co_3O_4/CC composite was dried for 12 h in a vacuum oven at 80°C. After 2 h of carbonization in a N_2 tube furnace at 550°C and the heating rate of 5°C min^{-1}, the corresponding NC–Co_3O_4/CC-600, NC–Co_3O_4/CC-900, and NC–Co_3O_4/CC-1200 composites were obtained.

Characterizations

Scanning electron microscopy (SEM) images were obtained with a Hitachi S-4800 instrument operating at 5 kV. Transmission electron microscopy (TEM) imaging was performed on a JEM-2100 electron microscope (JEOL) with an acceleration voltage of 200 kV. X-ray diffraction (XRD) patterns were collected on a Rigaku D/max-IIIB diffractometer, using Cu Kα radiation (λ = 1.5406 Å) with an acceleration voltage of 40 kV and applied current of 20 mA. Raman spectra were obtained on a Jobin Yvon HR800 micro-Raman spectrometer at 457.9 nm. X-ray photoelectron spectroscopy (XPS) was conducted with a Mg Kα achromatic X-ray source.

Electrochemical tests

OER tests were performed with a standard three-electrode system on a CHI660 electrochemical workstation at 25°C. The synthetic self-supported composite, a Pt foil and the SCE were used as the working electrode, the counter electrode, and the reference electrode, respectively. Linear scan voltammetry (LSV) curves were acquired in an O_2-saturated 1.0 mol L^{-1} KOH electrolyte with a scanning speed of 5 mV s^{-1}. In all measurements, the SCE reference electrode was calibrated in 1.0 mol L^{-1} KOH electrolyte with reversible hydrogen electrode (RHE) in accordance with the formula E(RHE)=E(SCE)+ 1.059 V. All LSV curves were treated by *iR* correction. The endogenously manufactured Zn-air battery was assembled as follows: the synthetic self-supported composite was used as an air cathode, a polished zinc plate was used as the anode, and 6.0 mol L^{-1} KOH+ 0.2 mol L^{-1} $Zn(CH_3COO)_2$ were used as the electrolyte. The gas diffusion area was 1 cm^2 to allow ambient O_2 come in contact with the catalyst active sites. All the

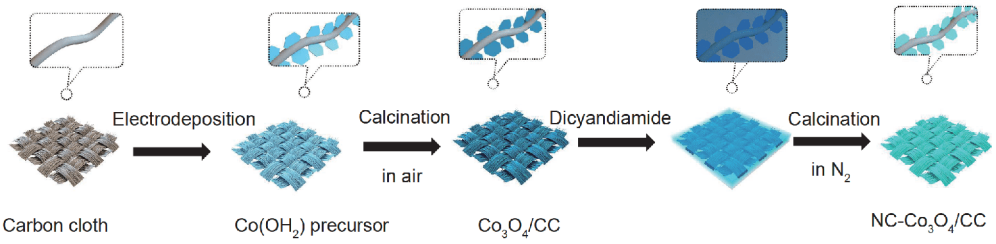

Scheme 1 Synthetic scheme of NC-Co_3O_4/CC.

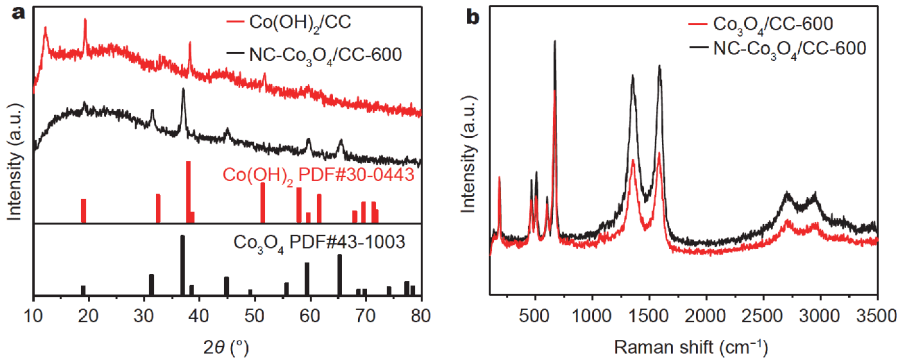

Figure 1 (a) XRD patterns of $Co(OH)_2$/CC and NC-Co_3O_4/CC-600. (b) Raman spectra of of Co_3O_4/CC-600 and NC-Co_3O_4-600.

batteries were tested in the atmospheric environment using LAND CT2001A multichannel battery test system. The charge-discharge cycle comprised a 30 min discharge followed by a 30 min charge.

RESULTS AND DISCUSSION

Morphological and structural characterization

The synthesis of NC–Co_3O_4/CC is shown in Scheme 1. First, $Co(OH)_2$ nanosheets grown on CC were synthesized through electrochemical deposition in $Co(NO_3)_2$ solutions. Then, the $Co(OH)_2$ phase was converted to Co_3O_4 after calcination in air, immersed in diamine solution, immersed in dicyandiamide solution, and then carbonized to yield the NC–Co_3O_4/CC composite. Approximately 2.7 mg cm^2 NC–Co_3O_4 was loaded on NC–Co_3O_4/CC-600. The crystal phase of the synthetic composite was first assessed on the basis of XRD patterns. As shown in Fig. 1a, the spectra of the $Co(OH)_2$/CC sample showed distinct diffraction peaks at 2θ = 19.1°, 37.9°, 51.3°, 57.9°, and 61.5° that correspond to the (001), (101), (102), (110), and (111) planes of β-$Co(OH)_2$ (PDF#30-0443), respectively. The diffraction peaks at 2θ = 19.0°, 31.3°, 36.9°, 44.8°, 59.4° and 65.3° in the spectra of the NC–Co_3O_4/CC-600 sample were attributed to the (111), (220), (311), (400), (511) and (440) planes of the face-centered cubic spinel, i.e., Co_3O_4 (PDF#43-1003), respectively [43]. The crystalline phases of the NC–Co_3O_4/CC-900 and NC–Co_3O_4/CC-1200 composites were similar to those of NC–Co_3O_4/CC-600 (Fig. S1). Raman spectroscopy is a useful technology for investigating the graphization degree of carbon nanostructures. As shown in Fig. 1b, the G-band peak at 1,594 cm^{-1} was attributed to the in-plane bond-stretching motion of sp^2 carbon atoms. The D-band peak at 1,348 cm^{-1} originated from the structural defects of sp^3 carbon atoms. The G-band and D-band (I_G/I_D) intensity ratio of NC–Co_3O_4/CC-600 was higher than that of Co_3O_4/CC-600. This result indicates that NC–Co_3O_4/CC-600 has high graphitization degree and could provide numerous active sites [44].

The morphology and nanostructures of the starting materials, intermediate structures, and final electrodes were characterized in detail through SEM and TEM. Fig. S2a, b show that the blank CC contained a smooth surface. The $Co(OH)_2$ nanosheet array had uniformly and vertically grown on the CC substrate after electrochemical deposition (Fig. 2a–c). This growth pattern could result in the construction of a 3D network. After calcination and carbonization, the structures of Co_3O_4/CC (Fig. 2d) and NC–Co_3O_4/CC-600 (Fig. 2e, f) became similar to those of $Co(OH)_2$. These structures can favor electron transport and enhance electrochemical performance. When the

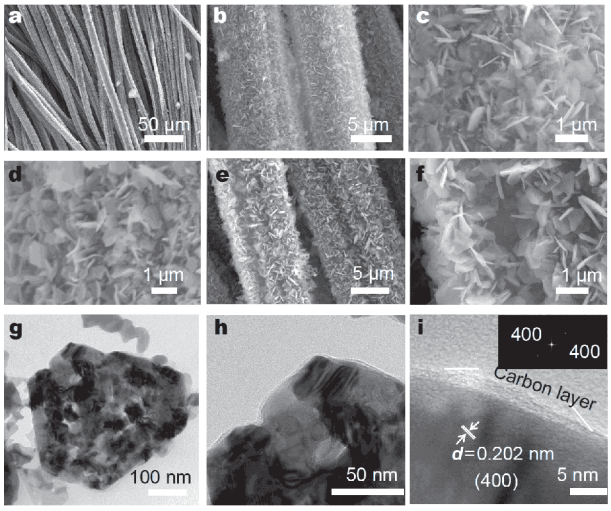

Figure 2 SEM images of (a–c) $Co(OH)_2$/CC, (d) Co_3O_4/CC, (e, f) NC-Co_3O_4/CC-600; (g, h) TEM and (i) HRTEM images of NC-Co_3O_4/CC-600 (inset is the corresponding FT).

duration of electrochemical deposition increased from 600 s to 900 s, most of the Co_3O_4 nanosheets in the NC–Co_3O_4/CC-900 on the surface of CC substrate became flattened (Fig. S2c, d). After 1,200 s, the morphology of the NC–Co_3O_4/CC-1200 sample became irregular (Fig. S2e, f)). As shown in Fig. S3a, Co_3O_4/CC-600 exhibited a hexagonal lamellar structure with a diameter of approximately 250–260 nm. The high-resolution TEM (HRTEM) image presented in Fig. S3b shows a set of clear lattice fringe with a spacing of 0.233 nm that corresponded to the (222) plane of Co_3O_4. Fig. 2g shows that NC–Co_3O_4/CC exhibited a hexagonal lamellar structure with a diameter of approximately 300–310 nm, and the hexagonal lamella had a thin film structure on the edge (Fig. 2h). The group of lattice fringes with a spacing of 0.202 nm shown in Fig. 2i was ascribed to the (400) faces of Co_3O_4 (Fig. 2i). The corresponding Fourier transform (FT) image in the inset of Fig. 2i further confirmed the existence of (400) planes in the lattice fringes. In addition, the Co_3O_4 nanosheet was coated with an amorphous carbon layer that could improve electron transfer and promote OER performance.

XPS analysis was performed to further confirm the chemical composition and valence state of the synthetic samples. As shown in Fig. S4, the wide XPS survey spectra indicates the presence of elemental Co, O, N, and C in NC–Co_3O_4/CC, whereas the elemental Co, O, and C existed in Co_3O_4/CC. The content of N in NC-Co_3O_4/CC is about 1.9 at.% derived from dicyandiamide. The high-resolution XPS spectrum of Co 2p for NC–Co_3O_4/CC-600 is shown in Fig. 3a. The two peaks centered at 780.3 and 795.5 eV corresponded to Co $2p_{3/2}$ and Co $2p_{1/2}$, respectively. Co $2p_{3/2}$ could be further divided into two peaks at 780.5 and 779.4 eV that respectively corresponded to Co^{3+} and Co^{2+}. Meanwhile, Co $2p_{1/2}$ could be divided into two peaks at 795.0 and 796.8 eV that originated from Co^{3+} and Co^{2+}, respectively. Co^{3+} and Co^{2+} existed in the catalyst. The peak at 784.9 eV was attributed to Co–N_x bonds. Meanwhile, the two satellite peaks (sat.) at 789.4 and 804.1 eV had a combined energy difference of 14.7 eV. Moreover, the high Co^{3+}/Co^{2+} ratio of NC–Co_3O_4/CC-600 indicates that Co^{3+} content could be attributed to the doping of elemental N, which is beneficial for catalytic water cracking and improving OER performance [45]. The C 1s spectrum provided in Fig. 3b could be divided into C–C (284.6 eV), C–N (285.8 eV), C=O (288.3 eV), and π–π^* (291.7 eV) peaks [46]. The existence of the C–N bond indicates that the N atoms had been doped into the carbon network and demonstrates the formation of N-doped amorphous carbon. The XPS spectrum of N 1s in Fig. 3c can be deconvoluted into two characteristic peaks: Co–N at 399.4 eV and graphitic N at 401.1 eV. The interactions of Co–N stablize compound electronic structure, and increase Co^{3+} content [47]. The O 1s spectrum in Fig. 3d shows that the two peaks at 530.0 and 531.1 eV were attributable to Co–O and oxygen vacancies, respectively. The existence of oxygen vacancies benefits oxygen adsorption and stabilizes oxygen absorbates. These effects increase the OER rate. The high-resolution XPS spectra of Co 2p and O 1s for NC–Co_3O_4/CC-900 and NC–Co_3O_4/CC-1200 are shown in Fig. S5. The Co^{3+}/Co^{2+} ratios of NC–Co_3O_4/CC-900 and NC–Co_3O_4/CC-1200 were 2.4 and 1.4, respectively, and were lower than that of NC–Co_3O_4/CC-600 (2.6). Moreover, the mass content of oxygen vacancies of NC–Co_3O_4/CC-600, NC–Co_3O_4/CC-900, and NC–Co_3O_4/CC-1200 were approximately 10.4%, 9.5%, and 7.4%, respectively. These results demonstrate that the oxygen vacancy contents and Co^{3+}/Co^{2+} ratios of the samples decreased with the increase in electrodeposition duration as illustrated by the XPS spectra shown in Fig. S5a and c. In other words, the oxygen vacancy contents and Co^{3+}/Co^{2+} ratios of the samples could be controlled by changing the electrodeposition time.

Electrocatalytic activity for OER and ORR

The OER performance of NC–Co_3O_4/CC-600 was first estimated in O_2-saturated 1.0 mol L^{-1} KOH electrolyte with a conventional three-electrode system. RuO_2 on CC (RuO_2/CC, RuO_2 loading of 2.7 mg cm^{-2}), Co_3O_4/CC-

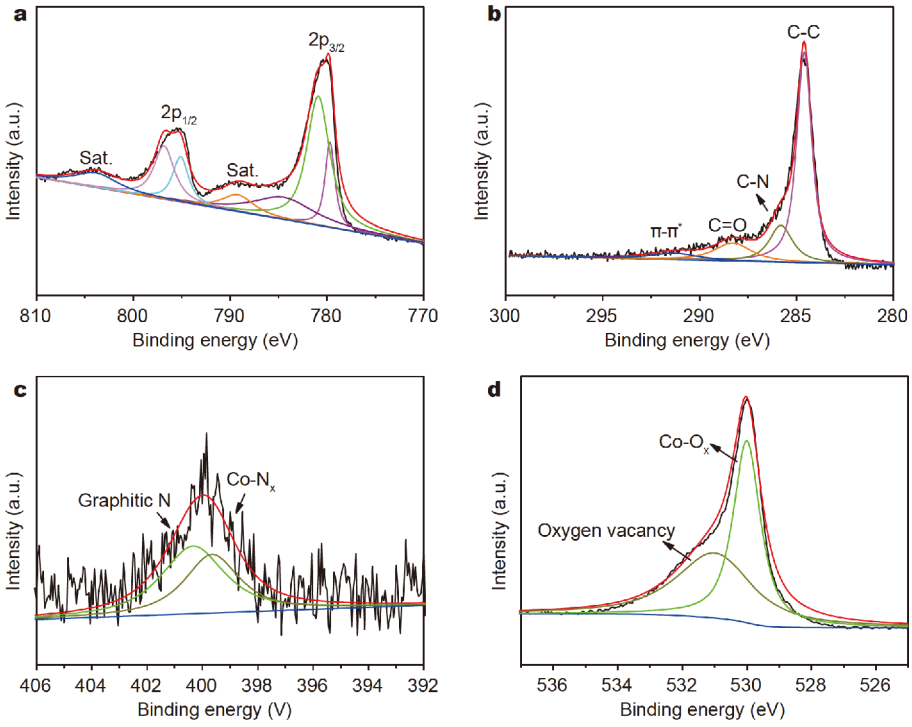

Figure 3 High-resolution XPS spectra of (a) Co 2p, (b) C 1s, (c) N 1s and (d) O 1s for NC-Co_3O_4/CC-600.

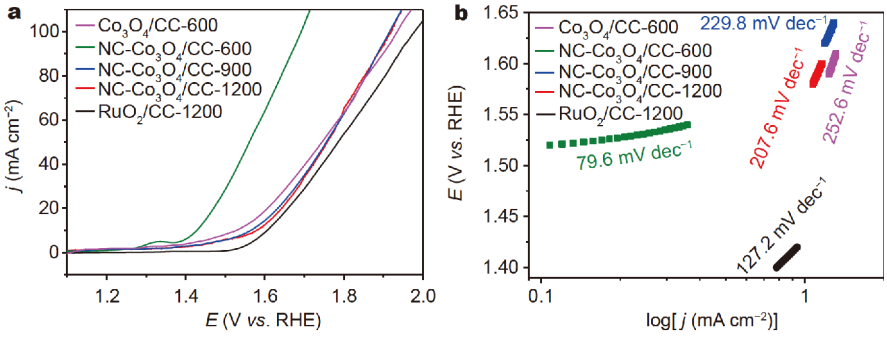

Figure 4 OER electrochemical performances: (a) LSV curves at a scan rate of 5 mV s^{-1} and (b) the corresponding Tafel plots of Co_3O_4/CC-600, NC-Co_3O_4/CC-600, NC-Co_3O_4/CC-900, NC-Co_3O_4/CC-1200 and RuO_2/CC catalysts.

600, NC–Co_3O_4/CC-600, NC–Co_3O_4/CC-900, NC–Co_3O_4/CC-1200 were also tested for comparison. The LSV curves of all samples are summarized in Fig. 4a. NC–Co_3O_4/CC-600 exhibited the best OER performance and only required an overpotential of 210 mV to drive a current density of 10 mA cm^{-2}. Conversely, Co_3O_4/CC-600, NC–Co_3O_4/CC-900, NC–Co_3O_4/CC-1200, and RuO_2/CC required overpotentials of 298, 334, 350, and 376 mV, respectively, to achieve the same current density. The reaction kinetics of OER on these catalysts were further inferred from the Tafel slope, which could be fitted to $\eta = a+b\log j$, where b is the Tafel slope and j is the corresponding current density. As shown in Fig. 4b, the Tafel slope of NC–Co_3O_4/CC-600 (79.6 mV dec^{-1}) was considerably lower than that of Co_3O_4/CC-600 (252.6 mV dec^{-1}), NC–Co_3O_4/CC-900 (229.8 mV dec^{-1}), NC–Co_3O_4/CC-1200 (207.6 mV dec^{-1}), and RuO_2/CC (127.2 mV dec^{-1}). These results reflect the fast reaction kinetics of the OER on NC–Co_3O_4/CC-600. The excellent OER catalytic activity of NC–Co_3O_4/CC-600 was attributed to its special 3D structures, which were composed of nanosheets that provided additional

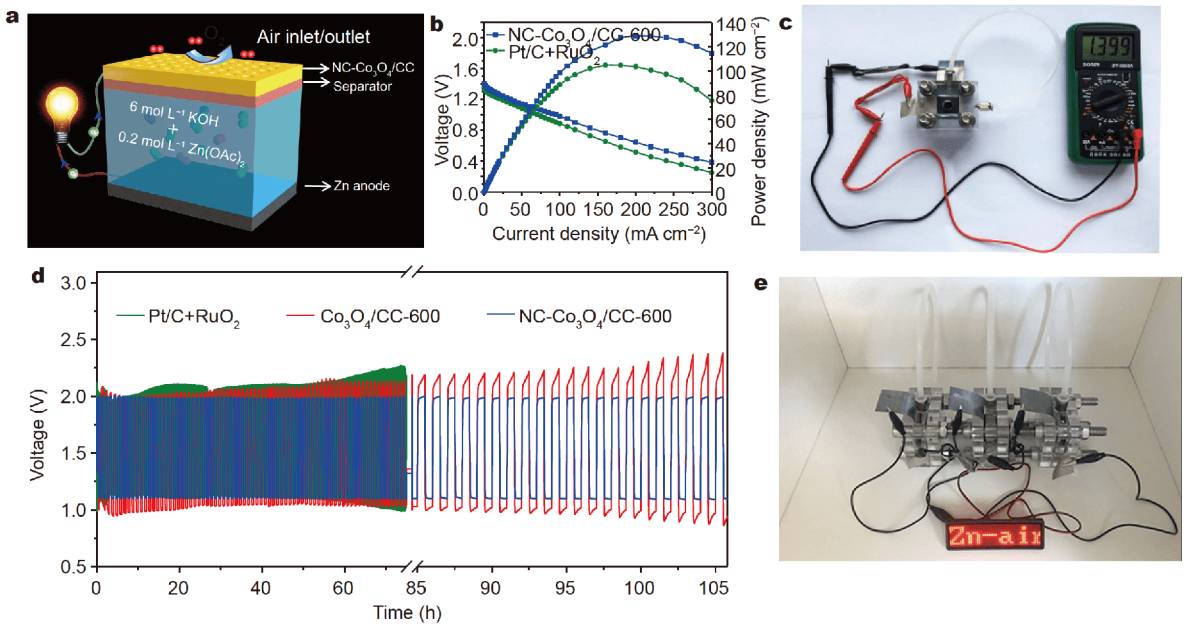

Figure 5 (a) Scheme of the rechargeable Zn-air battery. (b) Battery voltage and power density of rechargeable Zn-air batteries with NC-Co_3O_4/CC-600 and mixture of Pt/C+RuO_2 as air-cathodes in 6.0 mol L^{-1} KOH containing 0.2 mol L^{-1} $Zn(Ac)_2$ solution. (c) Open circuit voltage of the rechargeable Zn-air batteries with NC-Co_3O_4/CC-600 as air-cathodes. (d) Galvanostatic discharge-charge cycling curves at 10 mA cm^{-2} of rechargeable Zn-air batteries with the NC-Co_3O_4/CC-600, Co_3O_4/CC-600 and the mixture of Pt/C+RuO_2 as air-cathodes, respectively. (e) Photograph of a red LED indicator powered by three rechargeable Zn-air batteries with the NC-Co_3O_4/CC-600 as air-cathode in series.

reaction active sites and promoted electron/ion transfer. These effects enhanced the OER rate.

The LSV curves of the samples toward ORR acquired in 0.1 mol L^{-1} KOH are shown in Fig. S6. The onset (E_{onset}) and half-wave ($E_{1/2}$) potentials are important criteria for evaluation of ORR performance. NC–Co_3O_4/CC-600 exhibited higher E_{onset} and half-wave ($E_{1/2}$) potentials than the NC–Co_3O_4/CC-900 and NC–Co_3O_4/CC-1200 catalysts. The E_{onset} and $E_{1/2}$ potentials of NC–Co_3O_4/CC-600 were comparable with those of a commercial 20% Pt/C catalyst. The superior electrochemical performance of NC–Co_3O_4/CC-600 could be attributed to its moderate Co_3O_4 content, oxygen vacancy, and Co^{3+}/Co^{2+} ratios.

Zn-air battery performance

To evaluate the practicability of NC–Co_3O_4/CC-600, an endogenous rechargeable Zn-air battery was assembled with 6.0 mol L^{-1} KOH containing 0.2 mol L^{-1} $Zn(Ac)_2$ as an electrolyte, a polished Zn plate as an anode, and NC–Co_3O_4/CC-600 as an air cathode (Fig. 5a). For comparison, a commercial mixed catalyst of 20% Pt/C +RuO_2 (mass ratio of 1:1) and Co_3O_4/CC-600 were used as air cathodes in rechargeable Zn-air batteries and tested under the same conditions. As shown in Fig. 5b, the power density delivered by the NC–Co_3O_4/CC-600-enabled battery (129.08 mW cm^{-2}) was higher than that delivered by the commercial 20% Pt/C+RuO_2-enabled battery (104.86 mV cm^{-2}). The open-circuit voltage of the NC–Co_3O_4/CC-600 enabled battery was 1.399 V as tested by a multimeter (Fig. 5c). A long-cycle charge-discharge experiment was conducted at the current density of 10 mA cm^{-2} to evaluate the performance and stability of the Zn-air battery used in the experiment. Each cycle was discharged for 30 min and then charged for 30 min. As shown in Fig. 5d, the initial discharge and charge voltages of the NC–Co_3O_4/CC-600-enabled battery were 1.10 and 1.97 V, respectively. The voltage gap between the discharging and charging of the NC–Co_3O_4/CC-600-based battery was 0.87 V, which was significantly lower than that of the Co_3O_4/CC-600- and Pt/C+RuO_2-based battery. The stable voltage gap demonstrated by the NC–Co_3O_4/CC-600-based battery over 106 cycles suggests that NC–Co_3O_4/CC-600 has excellent stability. The superior activity, stability, and voltage gaps of the other two kinds of NC–Co_3O_4/CC-600 over those of Co_3O_4/CC-600 demonstrate that electrochemical performance could be improved by the N-doped carbon coating on Co_3O_4.

Furthermore, the fine stability exhibited by the NC–Co_3O_4/CC-600-based battery at a large current density of 25 mA cm^{-2} over 93 cycles (voltage difference is 1.12 V,

Fig. S7) indicates its potential applications in high-power supply systems. Given the exceptional charge-discharge performance and long-cycle stability of the NC–Co_3O_4/CC-600-enabled Zn-air battery, its potential in practice should be explored. As shown in Fig. 5e, three Zn-air batteries in series could provide power to a red LED viewing screen (2.7 V) for at least 24 h of illumination. This result suggests that the present NC–Co_3O_4/CC-600 is a productive air cathode material for rechargeable Zn-air batteries. The special structure of the self-supported electrode provides the followed advantages: (i) the 3D structures increase the surface area and facilitate diffusion and transfer of electrolyte ions and electrons; (ii) the introduction of the N atom adjusts the structure of the C electron and accelerates the transfer of electrons; (iii) the carbon coating could improve the electrochemical stability and enhanced catalytic activity resulting from the absence of a binder.

CONCLUSIONS

A 3D NC–Co_3O_4/CC electrode composed of N-doped carbon-coated Co_3O_4 nanosheets grown on CC was successfully fabricated *via* a facile and effective strategy. When used as a binder-free self-supported electrode, the NC–Co_3O_4/CC electrode required an overpotential of 210 mV to achieve the current density of 10 mA cm^{-2} and a Tafel slope of 79.6 mV dec^{-1}. The Zn-air battery test showed that the NC–Co_3O_4/CC electrode had a smaller charge/discharge voltage gap and better durability than a commerical Pt/C+RuO_2 electrode mixture. The high catalytic performance of the NC–Co_3O_4/CC electrode could be attributed to the synergistic effect of the 3D structures, N-doped carbon coating, and Co_3O_4 nanosheets on catalytic activity. This study would stimulate the research on the use of self-supported materials with various components and nanostructures as metal-air batteries.

Received 3 September 2018; accepted 24 September 2018; published online 5 November 2018

1 Liang Y, Li Y, Wang H, *et al.* Strongly coupled inorganic/nanocarbon hybrid materials for advanced electrocatalysis. J Am Chem Soc, 2013, 135: 2013–2036
2 Fu J, Cano ZP, Park MG, *et al.* Electrically rechargeable zinc-air batteries: progress, challenges, and perspectives. Adv Mater, 2017, 29: 1604685
3 Xiao Y, Tian C, Tian M, *et al.* Cobalt-vanadium bimetal-based nanoplates for efficient overall water splitting. Sci China Mater, 2018, 61: 80–90
4 Dresselhaus MS, Thomas IL. Alternative energy technologies. Nature, 2001, 414: 332–337
5 Yang Y, Luo M, Xing Y, *et al.* A universal strategy for intimately coupled carbon nanosheets/MoM nanocrystals (M = P, S, C, and O) hierarchical hollow nanospheres for hydrogen evolution catalysis and sodium-ion storage. Adv Mater, 2018, 30: 1706085
6 Li G, Wang X, Fu J, *et al.* Pomegranate-inspired design of highly active and durable bifunctional electrocatalysts for rechargeable metal-air batteries. Angew Chem Int Ed, 2016, 55: 4977–4982
7 Wang XR, Liu JY, Liu ZW, *et al.* Identifying the key role of pyridinic-N-Co bonding in synergistic electrocatalysis for reversible ORR/OER. Adv Mater, 2018, 30: 1800005
8 Wang Z, Jia W, Jiang M, *et al.* Microwave-assisted synthesis of layer-by-layer ultra-large and thin NiAl-LDH/RGO nanocomposites and their excellent performance as electrodes. Sci China Mater, 2015, 58: 944–952
9 Yang C, Feng J, Lv F, *et al.* Metallic graphene-like VSe_2 ultrathin nanosheets: superior potassium-ion storage and their working mechanism. Adv Mater, 2018, 30: 1800036
10 Hu S, Han T, Lin C, *et al.* Enhanced electrocatalysis *via* 3D graphene aerogel engineered with a silver nanowire network for ultrahigh-rate zinc-air batteries. Adv Funct Mater, 2017, 27: 1700041
11 Park J, Risch M, Nam G, *et al.* Single crystalline pyrochlore nanoparticles with metallic conduction as efficient bi-functional oxygen electrocatalysts for Zn–air batteries. Energy Environ Sci, 2017, 10: 129–136
12 Chen B, He X, Yin F, *et al.* MO-Co@N-doped carbon (M = Zn or Co): vital roles of inactive Zn and highly efficient activity toward oxygen reduction/evolution reactions for rechargeable Zn-air battery. Adv Funct Mater, 2017, 27: 1700795
13 Cui Z, Fu G, Li Y, *et al.* Ni_3FeN-supported Fe_3Pt intermetallic nanoalloy as a high-performance bifunctional catalyst for metal-air batteries. Angew Chem Int Ed, 2017, 56: 9901–9905
14 Pei Z, Li H, Huang Y, *et al.* Texturing *in situ*: N,S-enriched hierarchically porous carbon as a highly active reversible oxygen electrocatalyst. Energy Environ Sci, 2017, 10: 742–749
15 Song F, Hu X. Ultrathin cobalt–manganese layered double hydroxide is an efficient oxygen evolution catalyst. J Am Chem Soc, 2014, 136: 16481–16484
16 Wei L, Karahan HE, Zhai S, *et al.* Amorphous bimetallic oxide-graphene hybrids as bifunctional oxygen electrocatalysts for rechargeable Zn-air batteries. Adv Mater, 2017, 29: 1701410
17 Li Y, Yin J, An L, *et al.* Metallic $CuCo_2S_4$ nanosheets of atomic thickness as efficient bifunctional electrocatalysts for portable, flexible Zn-air batteries. Nanoscale, 2018, 10: 6581–6588
18 Wu J, Ren Z, Du S, *et al.* A highly active oxygen evolution electrocatalyst: Ultrathin CoNi double hydroxide/CoO nanosheets synthesized *via* interface-directed assembly. Nano Res, 2016, 9: 713–725
19 Chu Y, Guo L, Xi B, *et al.* Embedding MnO@Mn_3O_4 nanoparticles in an N-doped-carbon framework derived from Mn-organic clusters for efficient lithium storage. Adv Mater, 2018, 30: 1704244
20 Hwang S, Meng Q, Chen PF, *et al.* Strain coupling of conversion-type Fe_3O_4 thin films for lithium ion batteries. Angew Chem Int Ed, 2017, 56: 7813–7816
21 Wang J, Li K, Zhong H, *et al.* Synergistic effect between metal-nitrogen-carbon sheets and NiO nanoparticles for enhanced electrochemical water-oxidation performance. Angew Chem Int Ed, 2015, 54: 10530–10534
22 Wang L, Chen H, Daniel Q, *et al.* Promoting the water oxidation catalysis by synergistic interactions between $Ni(OH)_2$ and carbon

nanotubes. Adv Energy Mater, 2016, 6: 1600516
23 Wu D, Wei Y, Ren X, *et al.* $Co(OH)_2$ nanoparticle-encapsulating conductive nanowires array: room-temperature electrochemical preparation for high-performance water oxidation electrocatalysis. Adv Mater, 2018, 30: 1705366
24 Han A, Chen H, Sun Z, *et al.* High catalytic activity for water oxidation based on nanostructured nickel phosphide precursors. Chem Commun, 2015, 51: 11626–11629
25 Fenton JL, Schaak RE. Structure-selective cation exchange in the synthesis of zincblende MnS and CoS nanocrystals. Angew Chem Int Ed, 2017, 56: 6464–6467
26 Yin J, Li Y, Lv F, *et al.* Oxygen vacancies dominated NiS_2/CoS_2 interface porous nanowires for portable Zn-air batteries driven water splitting devices. Adv Mater, 2017, 29: 1704681
27 Feng LL, Yu G, Wu Y, *et al.* High-index faceted Ni_3S_2 nanosheet arrays as highly active and ultrastable electrocatalysts for water splitting. J Am Chem Soc, 2015, 137: 14023–14026
28 Liu Y, Li Q, Si R, *et al.* Coupling sub-nanometric copper clusters with quasi-amorphous cobalt sulfide yields efficient and robust electrocatalysts for water splitting reaction. Adv Mater, 2017, 29: 1606200
29 Chen L, Jiang H, Hu Y, *et al. In-situ* growth of ultrathin MoS_2 nanosheets on sponge-like carbon nanospheres for lithium-ion batteries. Sci China Mater, 2018, 61: 1049–1056
30 Shen H, Gracia-Espino E, Ma J, *et al.* Atomically FeN_2 moieties dispersed on mesoporous carbon: A new atomic catalyst for efficient oxygen reduction catalysis. Nano Energy, 2017, 35: 9–16
31 Amiinu IS, Liu X, Pu Z, *et al.* From 3D ZIF nanocrystals to Co-N_x/C nanorod array electrocatalysts for ORR, OER, and Zn-air batteries. Adv Funct Mater, 2018, 28: 1704638
32 Cai P, Hong Y, Ci S, *et al. In situ* integration of CoFe alloy nanoparticles with nitrogen-doped carbon nanotubes as advanced bifunctional cathode catalysts for Zn–air batteries. Nanoscale, 2016, 8: 20048–20055
33 Tan P, Chen B, Xu H, *et al.* Co_3O_4 nanosheets as active material for hybrid Zn batteries. Small, 2018, 14: 1800225
34 Li X, Wu H, Elshahawy AM, *et al.* Cactus-like NiCoP/NiCo-OH 3D architecture with tunable composition for high-performance electrochemical capacitors. Adv Funct Mater, 2018, 28: 1800036
35 Jiang H, Liu Y, Li W, *et al.* Co nanoparticles confined in 3D nitrogen-doped porous carbon foams as bifunctional electrocatalysts for long-life rechargeable Zn-air batteries. Small, 2018, 14: 1703739
36 Xue Y, Ren Z, Xie Y, *et al.* $CoSe_x$ nanocrystalline-dotted CoCo layered double hydroxide nanosheets: a synergetic engineering process for enhanced electrocatalytic water oxidation. Nanoscale, 2017, 9: 16256–16263
37 Cui Z, Li Y, Fu G, *et al.* Robust Fe_3Mo_3C supported IrMn clusters as highly efficient bifunctional air electrode for metal-air battery. Adv Mater, 2017, 29: 1702385
38 Meng F, Zhong H, Bao D, *et al. In situ* coupling of strung Co_4N and intertwined N–C fibers toward free-standing bifunctional cathode for robust, efficient, and flexible Zn–air batteries. J Am Chem Soc, 2016, 138: 10226–10231
39 Yuan S, Huang X, Ma D, *et al.* Engraving copper foil to give large-scale binder-free porous CuO arrays for a high-performance sodium-ion battery anode. Adv Mater, 2014, 26: 2273–2279
40 Qu S, Song Z, Liu J, *et al.* Electrochemical approach to prepare integrated air electrodes for highly stretchable zinc-air battery array with tunable output voltage and current for wearable electronics. Nano Energy, 2017, 39: 101–110
41 Song Z, Han X, Deng Y, *et al.* Clarifying the controversial catalytic performance of $Co(OH)_2$ and Co_3O_4 for oxygen reduction/evolution reactions toward efficient Zn–air batteries. ACS Appl Mater Interfaces, 2017, 9: 22694–22703
42 Chen X, Liu B, Zhong C, *et al.* Ultrathin Co_3 O_4 layers with large contact area on carbon fibers as high-performance electrode for flexible zinc-air battery integrated with flexible display. Adv Energy Mater, 2017, 7: 1700779
43 Guan C, Sumboja A, Wu H, *et al.* Hollow Co_3O_4 nanosphere embedded in carbon arrays for stable and flexible solid-state zinc-air batteries. Adv Mater, 2017, 29: 1704117
44 Tang C, Wang B, Wang HF, *et al.* Defect engineering toward atomic Co-N_x-C in hierarchical graphene for rechargeable flexible solid Zn-air batteries. Adv Mater, 2017, 29: 1703185
45 Cheng H, Li ML, Su CY, *et al.* Cu-Co bimetallic oxide quantum dot decorated nitrogen-doped carbon nanotubes: a high-efficiency bifunctional oxygen electrode for Zn-air batteries. Adv Funct Mater, 2017, 27: 1701833

Acknowledgements We acknowledge the support from the National Natural Science Foundation of China (21631004, 21771059 and 21571054), and Heilongjiang Provincial Postdoctoral Science Foundation (LBH-Q16194).

Author contributions Liu Q designed and performed the experiments; Liu X, Yu P and Tian C analyzed partial experimental data. Wang L and Fu H wrote the paper. All authors contributed to the general discussion.

Conflict of interest The authors declare no conflict of interest.

Supplementary information XRD, SEM. TEM, XPS and performance data for compared samples are available in the online version of the paper.

Qi Liu is currently an MSc candidate in inorganic chemistry under the supervision of Assistant Prof. Lei Wang and Prof. Honggang Fu at Heilongjiang Univesity. His research focuses on developing excellent catalyst materials of energy storage.

Lei Wang received his BSc degree in 2007 and MSc degree in 2010 from Heilongjiang University, China. In 2013, she received her PhD degree from Jilin University, China. Then, she joined Heilongjiang University as a lecturer. She became an assistant professor in 2015. Her research interest focuses on the carbon-based nanomaterials for Li-ion batteries, supercapacitors, fuel cells, metal-air batteries, and electrocatalysis.

Honggang Fu received his BSc degree in 1984 and MSc degree in 1987 from Jilin University, China. He joined Heilongjiang University as an assistant professor in 1988. In 1999, he received his PhD degree from Harbin Institute of Technology, China. He became a full professor in 2000. Currently, he is a Cheung Kong Scholar Professor. His research interest focuses on the oxide-based nanomaterials for solar energy conversion and photocatalysis, the carbon-based nanomaterials for energy conversion and storage, and electrocatalysis.

N掺杂碳包覆的Co_3O_4纳米片/碳布复合材料用于稳定的可充电Zn空气电池

刘奇, 王蕾*, 刘旭, 于鹏, 田春贵, 付宏刚*

摘要 多种非贵金属化合物已经被用作锌空气电池的正极材料. 钴基自支撑电极由于其制备低成本、高性能的优势而具有良好的应用前景, 但是构建高效的钴基自支撑电极仍面临很大的挑战. 本研究中, 我们采用电沉积及后续碳化的方法制备了一种在碳布上生长的氮掺杂碳包覆Co_3O_4纳米片三维复合材料(NC-Co_3O_4/CC). 作为自支撑电极用作OER催化剂, 在电流密度为10 mA cm^{-2}时过电势为210 mV, Tafel斜率为79.6 mV dec^{-1}. 作为锌空气电池的正极材料时, 在10 mA cm^{-2}的电流密度下其充放电电压差为0.87 V, 即使大电流密度为25 mA cm^{-2}时仍然具有良好的稳定性(93次循环后性能没有衰减), 远远超过了商业催化剂. NC-Co_3O_4/CC电极优异的性能主要归因于三维结构利于电解液离子的扩散, 同时不使用粘结剂也能够增强电极的导电性. 另外, 碳包覆不仅能够提高电子传导特性, 而且能提升电极的电化学稳定性. 氮掺杂可以调节碳的电子结构, 加速电子的传递. 本工作提供了一种简单有效的策略用于合成各种自支撑电极, 从而满足不同能量存储及转换器件对电极的需求.

